Molecular approach to prepare mixed MoW alumina supported hydrotreatment catalysts using H4SiMonW12–nO40 heteropolyacids

Maria Nikulshina, Pascal Blanchard, Alexander Mozhaev, Christine Lancelot, Anne Constant, Michel Fournier, Edmond Payen, Olivier Mentre, Valérie Briois, Pavel Nikulshin, et al.

Journal Name

ARTICLE

Molecular approach to prepare mixed MoW alumina supported hydrotreatment catalysts using $H_4SiMo_nW_{12-n}O_{40}$ heteropolyacids

Received 00th January 20xx,
Accepted 00th January 20xx

DOI: 10.1039/x0xx00000x

www.rsc.org/

M. S. Nikulshina,[a,b] , P. Blanchard[a], A. Mozhaev[b], C. Lancelot[a], A. Griboval-Constant[a], M. Fournier[a], E. Payen[a], O. Mentré[a], V. Briois[c], P.A. Nikulshin[b]* and C. Lamonier[a]*

$H_4[SiMo_nW_{12-n}O_{40}]$ heteropolyacids (HPA) are interesting precursors for the preparation of alumina supported hydrotreating catalysts to introduce simultaneously both metals while maintaining a Mo-W nanoscale proximity. Two heteropolyacids with n = 1 and 3 have been synthesized and used for the first time for preparing hydrotreatment catalysts. The crystal structure refinement has been performed and evidences the formation of β-$H_4[SiMo_3W_9O_{40}]$ with three ordered Mo sites forming a face. The purity of the samples in aqueous solution has been shown from Raman and polarography characterizations. These heteropolyacids were then impregnated on alumina to prepare supported MoW based catalysts. As references, catalysts with same Mo/W ratios have been prepared using monometallic $H_4SiMo_{12}O_{40}$ and $H_4SiW_{12}O_{40}$ HPA (mixture of these 2 HPA in the impregnating solution). EXAFS characterization after drying performed simultaneously at the Mo K and W L_{III} edges indicate mixed heteropolyanion $SiMo_nW_{12-n}O_{40}^{4-}$ preservation at the alumina surface even if a partial decomposition to Keggin lacunary species could not be excluded and evidences after sulfidation the mixed "MoW-S_2" slabs formation. Better catalytic hydrogenation properties for dibenzothiophene hydrodesulfurization and naphthalene hydrogenation have been obtained when using β-$H_4[SiMo_3W_9O_{40}]$ which is explained by the formation of the mixed "MoW-S_2" active phase.

Introduction

The Keggin-type heteropolyanion or polyoxometallate (POM) $XM_{12}O_{40}^{n-}$ (with M = Mo, W and X a non-metallic atom) consists in a regular XO_4 tetrahedron surrounded by 12 MO_6 octahedra, which are connected by shared edges to form trimetallic M_3O_{13} groups joined together by their vertices[1]. Depending on the synthesis conditions, various isomers (as α,β,γ), obtained by a π/3 rotation of a M_3O_{13} group around C_3 axis, can be isolated[2]. At solid state, these ions and their counter-cations form a crystalline network, with a symmetry depending on the hydration of the solid and the nature of the counter-cation[2]. The "lacunary" Keggin structure corresponds to a Keggin structure in which one or more sites previously occupied by molybdenum or tungsten atoms are vacated. This new family corresponds to an M/X ratio of 11[3-5] or 9 [6,7], obtained by extracting one or three metal atoms from a single M_3O_{13} group or from different M_3O_{13} groups. These monovacant or polyvacant heteropolyanions can be synthesized directly depending on the medium pH. It is also possible to prepare substituted derivatives in which one or more metal atoms (Mo, W, etc.) of the dodeca-condensed structure are replaced by different atoms. Substitution can take place with an element whose oxidation number is much lower than that of the metal atom it is replacing (e.g. cobalt-II, nickel-II, iron-III…)[2,3], or with an element that can have similar properties to that of the substituted atom, as with vanadium-V in the case of the acid $H_4PMo_{11}VO_{40}$[8]. Sanchez et al.[9] have thereby isolated potassium and tetrabutyl ammonium salts of mixed $SiMo_1W_{11}O_{40}^{4-}$ and $SiMo_3W_9O_{40}^{4-}$ heteropolyanion. Reduction study on mono substituted Keggin $SiMo^{VI}_1W^{VI}_{11}$ synthesized with microtube shape has also been recently reported by Shen and al.[10] with the formation of stable reduced $SiMo^{V}_1W^{VI}_{11}$ microtube.

In the field of hydrotreatment catalysis, Keggin and Keggin-derivated heteropolymolybdate and heteropolytungstate structures have been successfully used to replace conventional precursors as ammonium heptamolybdate $(NH_4)_6Mo_7O_{24}$ (AHM) and ammonium metatungstate $(NH_4)_6H_2W_{12}O_{40}$ (AMT) to prepare oxidic precursors of metal sulfide catalysts[11-15]. From a catalytic point of view, the use of mixed metals Keggin-type POM may enhance activity due to the introduction of a second metal in the POM cluster. Mixed HPA precursors $PMo_{(12-x)}V_xO_{40}^{(3+x)-}$ generally used in the field of mild oxidation catalysis have been prepared for their use in hydrodemetallation catalysis[16] or diesel hydrotreatment[17]. The synthesis of cobalt salt of substituted $PCoMo_{11}O_{40}H^{6-}$ has been developed leading to HDS catalysts with improved catalytic performances compared to those of conventional catalysts prepared from AHM and cobalt nitrate[18]. For hydrocracking catalytic application, NiW ASA (Amorphous Silica Alumina) supported sulfide catalysts were also prepared from heteropolytungstate Ni salts as the substituted $Ni_3PW_{11}NiO_{40}H$ or the lacunary $Ni_4SiW_{11}O_{39}$ salt[12]. For

[a] Univ. Lille, CNRS, Centrale Lille, ENSCL, Univ. Artois, UMR 8181 - UCCS - Unité de Catalyse et Chimie du Solide, F-59000 Lille, France.
[b] Samara State Technical University, Molodogvardiyskaya st., Samara, 443100, Russia.
[c] Synchrotron SOLEIL, CNRS-UR1, BP 34, L'orme des Merisiers, Gif-sur-Yvette, France.
*p.a.nikulshin@gmail.com
*carole.lamonier@univ-lille1.fr

the CoMo system as well as for the NiW one, the vicinity of both elements in the HPA salt at the molecular level was able to generate a great amount of Co-MoS_2 or Ni-WS_2 active phase after sulfidation leading to improved catalytic performances[11,19].

Another way to develop active hydrotreating catalysts was carried out in 2001 with the use of bulk mixed tri-metallic (Ni)MoW sulfide. This new type of catalyst was at least three times more efficient than any previous hydrotreating catalyst, conventionally used in industry[20]. Further researches recently proposed to use less expensive MoW mixed supported catalysts prepared by impregnating on a support classical precursors (together or sequentially) such as ammonium heptamoybdate and ammonium metatungstate[21-23] or ammonium thiomolybdate $(NH_4)_2MoS_4$ and ammonium thiotungstate $(NH_4)_2WS_4$[24]. Mechanical mixture of supported NiMo-NiW catalysts has also been proposed[25]. Whatever the preparation procedure except mechanical mixture, Ni promoted mixed MoW catalysts revealed most of the time better catalytic performances than that of their monometallic counterpart.

We propose here a new approach to prepare MoW catalysts based on the use of mixed MoW heteropolyacids $H_4SiMo_nW_{12-n}O_{40}$, allowing to start from a single molecular entity to introduce together Mo and W. We synthesized two mixed heteropolyacids $H_4[SiMo_1W_{11}O_{40}]$ and $H_4[SiMo_3W_9O_{40}]$ that were extensively characterized at the solid state combining X-Ray Diffraction and XAS (X-Ray Absorption Spectroscopy) at the Mo K and W L_{III} edges. Purity of these mixed HPA together with their stability in aqueous solution was checked by Raman spectroscopy and polorography. Characterizations by Raman and XAS were also performed after deposition on alumina support in order to check the preservation of the mixed heteropolyacids. Catalytic results of the mixed supported system were compared to that obtained using monometallic $H_4SiMo_{12}O_{40}$ and $H_4SiW_{12}O_{40}$ HPA and their mixtures with Mo/W ratio = 1/11 and 3/9. Catalysts EXAFS characterization at the Mo K and W L_{III} edges after sulfidation have been used to explain the different hydrodesulfurization and hydrogenation properties.

Experimental

Synthesis of mixed $H_4[SiMo_nW_{12-n}O_{40}]$ heteropolyacids (HPA) (n=1,3)

α-$H_4[SiMo_1W_{11}O_{40}]$

In the first step, the lacunary Keggin polyoxotungstate potassium salt α-$K_8[SiW_{11}O_{39}]$ was prepared following reference[26]. 182 g of sodium tungstate (Na_2WO_4,$2H_2O$) and 11 g of silicate (Na_2SiO_3,$5H_2O$) were dissolved in 300 mL of hot water (60°C) in which was added 195 mL of hydrochloric acid (4M). After boiling this solution during one hour and cooling at room temperature (RT), the potassium salt was precipitated by solid KCl addition (about 50 g) and separated by filtration.

The synthesis of the potassium salt α-$K_4[SiMo_1W_{11}O_{40}]$ was then performed at RT following reference[9]. A MoO_2^{2+} molybdenum solution was prepared by addition of 6mL of nitric acid (13M) in 10 mL of a Na_2MoO_4 solution (1M). Then 10 g of α-$K_8[SiW_{11}O_{39}]$ were added by small fractions. The potassium salt of $SiMo_1W_{11}O_{40}^{4-}$ precipitated as a yellow solid. In order to allow better yield, it was filtered after 3 hours and purified by recrystallization in distilled water.

We observed that the mixed corresponding free acid was sufficiently stable to be crystallized from aqueous solution by using the "etherate" method[2]. A concentrated aqueous solution of the mixed MoW potassium salt was strongly acidified with HCl 12M and shaken with excess of diethyl oxide at RT. After separation, the heavy etherate phase was decomposed by addition of water. The remaining solution is let one night (around 12 hours) in a fume hood allowing vapor ether extraction. After removal of ether the aqueous solution was evaporated at 4 °C until α-$H_4[SiMo_1W_{11}O_{40}]$ heteropolyacid crystallization.

β-$H_4[SiMo_3W_9O_{40}]$

In the first step the lacunary Keggin polyoxotungstate sodium salt β-$Na_9[SiW_9O_{34}H]$ was prepared according to reference[27]. 12 g of sodium metasilicate (Na_2SiO_3, $5H_2O$) were dissolved in 250 mL of cold water (12°C) and 150 g of sodium tungstate (Na_2WO_4, $2H_2O$) were added. Hydrochloric acid (6M, 95 mL) was slowly added into the vigorously stirred solution. A silica residue was filtered off if necessary. The solution was left to stand at RT at least one hour while stirring and let in the fridge at 4°C during two days until precipitation.

The synthesis of the mixed potassium salt β-$K_8[SiMo_3W_9O_{39}]$ was performed following ref[9]. A MoO_2^{2+} molybdenum solution was prepared by addition of 60 mL of hydrochloric acid (12M) in 40 mL of a Na_2MoO_4 solution (1M). Then 27 g of β-$Na_9[SiW_9O_{34}H]$ were added by small fractions of 3 g. After 30 min, the resulting pale yellow solution was precipitated by 5 g of solid KCl to form $K_4[SiMo_3W_9O_{40}]$ that was filtered off.

The $H_4[SiMo_3W_9O_{40}]$ heteropolyacid is also prepared by dissolving the mixed potassium salt in water and extraction by ether and HCl. Crystals of β-$H_4[SiMo_3W_9O_{40}]$ were formed after evaporation at 4°C.

Preparation of the supported oxidic precursors

Impregnating solutions were prepared by dissolving mixed heteropolyacids in water solution. For comparison purposes, monometallic impregnating solutions were prepared using the Keggin heteropolyacids $H_4SiMo_{12}O_{40}$ and $H_4SiW_{12}O_{40}$ prepared according to references.[3,28] Bimetallic reference catalysts were also prepared using impregnating solutions obtained by mixing $H_4SiMo_{12}O_{40}$ and $H_4SiMo_{12}O_{40}$ in water solution with a Mo/W ratio of 1/11 and 3/9 corresponding to the mixed MoW heteropolyacids and were denoted Ref Mo_1W_{11} and Ref Mo_3W_9, respectively.

The oxidic precursors were prepared by incipient wetness impregnation of alumina support [γ-Al_2O_3 (Norton), specific area: 240 m^2/g, pore volume: 0.9 mL/g] with the aforementioned impregnating solutions.

In any case for comparison purpose, the HPA concentration was kept at 0.145 $mol_{HPA}.L^{-1}$ to set the (Mo+W) surface density at 3.9 atoms /nm^2, leading to different theoretical Mo/W loadings as reported in Table 1. All prepared impregnation solutions had a close pH value around 0.25 due to the same concentration of protons. After impregnation and 2 h of maturation in a wet atmosphere in order to let the species diffuse into the alumina extrudates, the solids were dried overnight at 100°C without further calcination.

Table 1. Composition of precursors and prepared catalysts.

Precursor(s)	Catalyst nomenclature	MoO_3 (wt %)	WO_3 (wt %)
$H_4SiMo_{12}O_{40}$	$SiMo_{12}/Al$	18.0	-
$H_4SiW_{12}O_{40}$	SiW_{12}/Al	-	26.2
$H_4SiMo_1W_{11}O_{40}$	$SiMo_1W_{11}/Al$	1.4	24.2
$H_4SiMo_3W_9O_{40}$	$SiMo_3W_9/Al$	4.2	20.1
$H_4SiMo_{12}O_{40}$+$H_4SiW_{12}O_{40}$	Ref Mo_1W_{11}	1.4	24.2
$H_4SiMo_{12}O_{40}$+$H_4SiW_{12}O_{40}$	Ref Mo_3W_9	4.2	20.1

Characterization techniques

Raman Spectroscopy

The Raman spectra of the samples were recorded at RT using an Infinity XY Horiba Jobin-Yvon Raman microprobe equipped with a photodiode array detector. The exciting laser source was the 532.16 nm line of a Nd-YAG laser. The wavenumber accuracy was 4 cm^{-1}.

TGA and DSC analysis

Thermogravimetric analysis was carried out with a STA 449 F3 Jupiter. The measurements were conducted in air with heating from RT to 600°C and a heating rate of 10°C/min. Samples of about 30 mg were introduced into a small corundum crucible, an empty crucible was used as the standard for thermal analysis.

Single crystal X-Ray Diffraction

Single crystals suitable for XRD experiments have been isolated from the crystallization products and sticked on a glass fiber using vacuum grease. Crystals of β-$H_4[SiMo_3W_9O_{40}].9H_2O$ are air stable and can be handled without precaution. On the opposite, crystals of the α-$H_4[SiMo_1W_{11}O_{40}].30H_2O$ are very unstable under exposure in air and rapidly decompose. In this case, crystals were placed in grease, rapidly mounted and the data were collected under nitrogen flow at 100 K without any decomposition.

Both crystal structures have been refined using single crystal XRD data collected on a DUO-Bruker SMART apex diffractometer using the Mo Kα radiation by least square minimization on F_{hkl}. Intensity data are corrected for Lorenz-Polarization effects and absorption, then the structure was solved and refined. Multiscan absorption correction was applied using SADABS[29]. The structure was solved using Superflip[30] and refined using Jana 2006[31]. Specificities for each collection and refinement are given below in the crystal structure dedicated sections. Further details of the crystal structures may be obtained from the Fachinformationszentrum Karlsruhe, 76344 Eggenstein-Leopoldshafen, Germany (Fax: +49-7247-808-666; e-mail: crysdata@fiz-karlsruhe.de, http://www.fiz-karlsruhe.de/request_for_deposited_data.html) on quoting the depository numbers CSD–431628 and CSD–431629 for the $SiMo_1W_{11}O_{40}H_4$ and $SiMo_3W_9O_{40}H_4$ hydrates, respectively. The quantification of the water molecules is discussed in the dedicated section.

X-Ray Absorption Spectroscopy

Mo K and W L_{III} edges EXAFS (Extended X-ray Absorption Fine Structure) measurements were carried out at the ROCK beamline of the SOLEIL synchrotron source[32] using Si(111) monochromator. The measurements were done at RT on powdery sample pressed into pellets when characterizing bulk HPA and dried catalysts at the oxide state. Sulfide catalysts were characterized after *in-situ* sulfidation using the catalytic cell available at SOLEIL [33]. Powdered dried oxide catalysts were loaded in the cell and the *in-situ* sulfidation was performed with a flow of 10% H_2S in H_2 at atmospheric pressure from RT to 400°C with a plateau of two hours according to the activation procedure applied in catalytic tests.

For the whole measurements, XAS spectra were obtained in transmission mode with ionization chambers as X-Ray detectors. The ionization chambers were filled with a mixture of argon and nitrogen (50:50) for measurements at the Mo K edge and (73:27) at the W L_{III} edge. Mo and W edges EXAFS regions of the spectra were extracted and analyzed using Athena and Artemis software packages[34]. For Mo K edge, $k^3\chi(k)$ EXAFS signals were Fourier transformed in R-space pseudo-radial distribution functions using a Kaiser−Bessel window between k_{min} = 4.8 $Å^{-1}$ and k_{max} = 10.5 $Å^{-1}$ and dk window sill parameter corresponding to the sloped region of Fourier transform is equal to 2. For W L_{III} edge, FT of the $k^3\chi(k)$ EXAFS data were carried out from 3.5 to 16.8 $Å^{-1}$ with a dk parameter equal to 2. The inverse Fourier Transformation of the EXAFS at the Mo K edge and W L_{III} edge were fitted using appropriate single and multiple scattering EXAFS

paths generated from the cif files derived from crystallographic structures. During fitting of mixed bulk samples using Artemis, the distances between the concerned atoms and the coordination numbers were constrained by the related parameters extracted from the XRD single crystal data to check the transferability of amplitude and phase functions which will be further applied for catalysts EXAFS analysis. In this frame, the amplitude reduction factor S_0^2, which takes into account multielectronic effects, together with the enot parameter which allows to match the k-scale of theoretical phase and amplitude functions with the one of the experimental EXAFS signals related to the user choice of the E_0 position on the edge, were first determined on the bulk HPA for the Mo and W edges. S_0^2 and enot values were after kept fixed for catalysts fitting. The number of fitted points was below the number of independent points according to the Nyquist criterion[35]. Typical accuracies for the determination of the coordination numbers and distances are 10 to 20 % and 1 to 2 %, respectively.

Polarography

The polarographic measurements were performed on a Tacussel (Pol 150) electrochemical analyzer monitored by a Tracemaster 5 programmer. A conventional single-compartment cell with standard three-electrodes configuration was used. Pt was used as an auxiliary electrode, while Ag/AgCl was used as a reference electrode. The working electrode was a glassy carbon disk (using a rate of stirring was equal to 840 rpm) allowing the heteropolymolybdates study with reduction waves observed in the range -0.1 and 0.5 V. Tungsten compounds being less reducible than molybdenum compounds, the study of $H_4SiW_{12}O_{40}$ that requires a mercury dropping electrode creating a higher overvoltage for reaching lower potential (between -1.1 and -0.2 V) could not be performed. Deoxygenating of the solutions was carried out using argon as inert gas. The concentration in molybdenum atoms was equal 10^{-3} M in aqueous electrolytic solutions HCl (1 M)/ethanol (equivolume).

XPS analysis

The composition and chemical state of the elements were studied using X-ray Photoelectron Spectroscopy (XPS) on a KRATOS Axis Ultra spectrometer equipped with a monochromatic Al Kα (1486.6 eV) X-ray radiation (powered at 100 watts). The analysis chamber was operated under ultrahigh vacuum with a pressure close 10^{-10} Torr. The binding energy (BE) values were referred to the Al_{2p} at 74.6 eV. Simulation of the experimental photopeaks was carried out using a mixed Gaussian/Lorentzian peak fit procedure according to the software supplied by *Casa XPS*. The methodology implemented for the decomposition of the Mo 3d and W4f spectra of the sulfided solids has been described elsewhere [12,36]. The Mo3d spectrum is decomposed in three doublets regarding Mo (three Mo species) and two S2s components associated to two sulfur species S^{2-} and $(S_2)^{2-}$ as usually reported for Mo(W) and Co(Ni)Mo hydrotreatment catalysts. The three well known Mo doublets whose $Mo3d_{5/2}$ components are placed at about 229.0, 230.5 and 233.0 eV according to three oxidation states of molybdenum, Mo^{IV}, Mo^{V} and Mo^{VI} respectively. The first contribution is attributed to MoS_2 phase, the second one is attributed to Mo^{V} surrounded by oxygen and sulfur atoms (intermediate sulfidation phase) and the contribution at higher binding energy is assigned to Mo^{VI} oxide species. The W4f spectra could also be decomposed into three doublets whose $W4f_{7/2}$ components are attributed to three different W species: W^{IV} sulfide (WS_2) with BE at about 32.2 eV), W^{V} oxysulfide with BE at about 33.5 eV and W^{VI} oxide with BE at about 36 eV. The decomposition of Mo3d and W4f XPS spectra allowed obtaining the relative atomic % of each corresponding Mo (W) species noted $\%Mo_i$ ($\%W_i$) according to the following formula:

$\%Mo_i = [A_i(Mo3d_{5/2} + Mo3d_{3/2}) / \sum(A_i(Mo3d_{5/2} + Mo3d_{3/2}))] \times 100$

where $A_i(Mo3d_{5/2} + Mo3d_{3/2})$ is the area of one Mo doublet,

and $\%W_i = [A_i(W4f_{7/2} + W4f_{5/2}) / \sum(A_i(W4f_{7/2} + W4f_{5/2}))] \times 100$

where $A_i(W4f_{7/2} + W4f_{5/2})$ is the area of one W doublet.

Catalytic activity

The catalytic properties were evaluated using a fixed-bed microreactor featuring a high-pressure flow system. 0.6 g of sieved catalyst (0.25 – 0.50 mm) was diluted with 1 cm^3 of low-surface-area sieved carborundum (0.2 – 0.4 mm) and placed in the centre of the reactor (the reactor had an internal diameter of 8 mm). Before testing, the catalysts were sulfided in a flow of 10% H_2S in H_2 at 400°C for 2 h. A mixture of DBT (1500 ppm S), naphthalene (3 wt. %), hexadecane (as an internal standard, 1 wt. %) and toluene (as a solvent) was used as a model feedstock for evaluation of HDS and hydrogenation (Hyd) performances. Catalysts were tested under the following conditions: 320°C, 3.0 MPa hydrogen, 10 h^{-1} liquid hourly space velocity (LHSV) and a 500 NL/L volume ratio of hydrogen to feed. The liquid product compositions of the samples collected every 0.5 h were determined using a Crystall-5000 Gas Chromatograph (GC) equipped with a 30 m OV-101 column. The reaction products were identified by matching retention times with those of commercially available standards and by GC/MS analysis using a Finnigan Trace DSQ. The HDS reaction was allowed to proceed for 12 h to evaluate the deactivation of the catalyst. However, all catalysts exhibited stable performance, achieving a steady state after 5 – 6 h. All catalysts were tested two times to exclude the possible error and average values of reactants conversion and selectivity ratios were calculated. The rate constants of the pseudo-first-order reactions of the DBT HDS and naphthalene Hyd were determined using the following equations:

$$k_{HDS} = -\frac{F_{DBT}}{w}\ln(1 - x_{DBT}) \qquad k_{Hyd} = -\frac{F_{Naph}}{w}\ln(1 - x_{Naph}), \quad (1)$$

where K_{HDS} and K_{Hyd} are the pseudo-first-order reaction constants for the DBT HDS and naphthalene Hyd (mol g^{-1} h^{-1}) respectively, X_{DBT} and x_{Naph} are the conversions (%) of DBT, and naphthalene respectively, F_{DBT} and F_{Naph} are the reactant flows in moles (mol h^{-1}) and *w* is the weight of the catalyst (g).

The HDS products from DBT include biphenyl (BP) via the direct desulfurization (DDS) pathway, as well as cyclohexylbenzene (CHB)

and bicyclohexyl (BCH) from the HYD pathway. The HYD/DDS selectivity was calculated according to the reaction network for DBT HDS (Scheme 1):

$$S_{HYD/DDS} = \frac{k_{HYD}}{k_{DDS}} = \frac{C_{CHB} + C_{BCH}}{C_{BP}}, \quad (2)$$

where C_{CHB}, C_{BCH}, and C_{BP} are the concentrations (wt. %) of CHB, BCH, and BP in the reaction products, respectively.

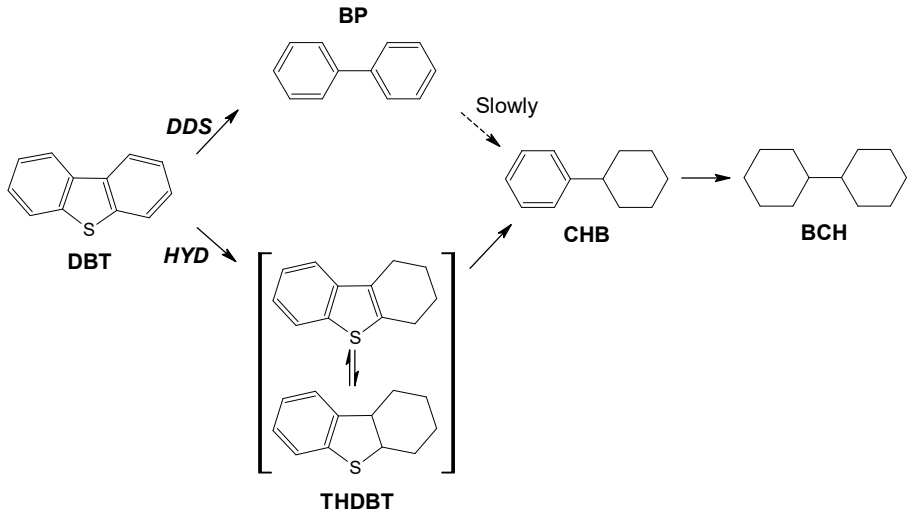

Scheme 1. Reaction network of the HDS of DBT.

Results and discussion

HPA Crystal Structures:

For both compounds, the space group was determined by means of the systematic extinctions and several models have been tested in case of ambiguities. The charge flipping method located most of the atoms with their chemical nature on the basis of their coordination and convergence of the refinement. Complementary anions, including water molecules have been located on Fourier-difference maps. They are often associated to large thermal parameters due to local disorder, e.g. Mo/W, protonation or not. To validate the presence of water molecules in between the polyanions, the occupancies of oxygen atoms (Ow) was refined and rejected if significantly lower than 100%. It means that the hydration rate given above stem from crystal refinements, but additional water molecules could exist in some partially occupied available voids. Collection and refinement parameters are given in Table 2. Intra HPA cation-anion bond distances are reported in SI (Table 1 SI).

Table 2. Crystal data, data collection and structure refinement parameters for single crystal of α-$H_4[SiMo_1W_{11}O_{40}]$ and β-$H_4[SiMo_3W_9O_{40}]$ poly-hydrates.

Formula	**α-$H_4[SiMo_1W_{11}O_{40}]\cdot 30H_2O$**	**β-$H_4[SiMo_3W_9O_{40}].9H_2O$**
Diffractometer: Bruker ApexII, Duo, λ =0.7107 Å (Mo Kα)		
Crystal System	Tetragonal	Monoclinic
Space group	P-4n2	$P2_1/m$
a (Å)	12.735(1)	10.1951(2)
b (Å)	-	14.4697(2)
c (Å)	18.079(1)	14.8556(2)
β(°)	-	100.3961(8)
V (Å^3)	2932.2(4)	2155.52(6)
Z	2	2
ρ_{calc} (g cm^{-3})	3.8133	4.28
μ (mm^{-1})	21.85	24.89
N collected Reflection	126997	29958
N ind Reflections (all)	3013	5729
R_{int} (%)	5.01	4.14

θ min-max	1.96-26.42	1.98-28.62
hkl range	15≥h≥-15	13≥h≥-13
	15≥h≥-15	19≥k≥-19
	22≥h≥-22	20≥l≥-19
Refinement method:	**Least squares on F**	
$R_1[I > 3\sigma(I)]^a$	0.0229	0.0284
$wR_2{}^a$	0.0239	0.0410
R_1 (all data)	0.0275	0.0439
wR_2	0.0276	0.0448
Weighting scheme	unit	unit
goodness-of-fit	0.43	1.92
N. refined parameters	175	176
largest diff. peak and hole [e Å^{-3}]	1.37, –1.12	2.64, –2.31

^{a} $R_1=\sum||F_o|-|F_c||/\sum|F_o|$; $wR_2=\{\sum[w(F_o^2-F_c^2)_2]/\sum[w(F_o^2)^2]\}^{1/2}$

α-$H_4[SiMo_1W_{11}O_{40}]$. 30 H_2O:

After data collection at 100K, the crystal structure was satisfactorily refined in the tetragonal P-4n2 symmetry. The lattice parameters and final R values are a= 12.735(1) Å, c=18.079(1) Å, Z= 2, R_{obs} =2.29%, wR_{all} =2.75%. The refinement of the statistic disorder over the three 8(i) general positions occupied by metal ions matches well the experimental predicted formula and was fixed to ideal Mo:W =1/12 : 11/12 in the last refinement cycles. Some external oxygen (O1, O5, O6) and water molecules have very large thermal parameters which mainly picture local disordering due to the statistic Mo/W disorder and distribution of bond lengths. Si-O distances are 1.624 Å while the three independent W/MoO_6 octahedra are typical with one short (~1.66 Å) four intermediate (~1.80-2.01 Å) and one long (~ 2.40 Å) bonds. The number of crystallization water molecules is important leading to separation between heteropolyanions around ~12.8 Å (measured from Si to Si), as shown Fig 1 (a). The morphology of the polyanion is typical of the α-form with four W_3O_{13} groups surrounding symmetrically (T_d symmetry) the SiO_4 tetrahedron. In each W_3O_{13} group, WO_6 octahedra are linked by edge-sharing while the octahedra belonging to two different $W_{13}O_{13}$ groups are sharing oxygen corners. From the $SiW_{12}O_{40}{}^{4-}$ structure any WO_6 can be removed and be replaced by one MoO_6 octahedron to form the lacunary $\alpha[SiW_{11}O_{39}]^{8-}$ structure. The announced 30 H_2O hydration amount was deduced from the water molecules present in a sufficient amount for refined occupancies greater than 30% and with viewable Debye Waller parameters and should approach rather well the true composition. It is clear that the local protonation of the external oxygen anions creates local off centering in the water sub-array.

β-$H_4[SiMo_3W_9O_{40}]$. 9 H_2O:

The crystal structure adopts the monoclinic $P2_1/m$ symmetry with lattice parameters and final R values a=10.1951(2) Å, b=14.4697(2) Å, c=14.8556(2) Å, β=100.3961(8)°, R_{obs} =2.84%, wR_{obs} =4.10%. In the solid, the polyanions are separated by ~9.6 Å leading to a much smaller hydration ratio than in the previous case. In this compound one rare characteristic concerns the full ordering detected between Mo and W sites. The β-$SiMo_3W_9O_{40}$ is obtained from a β-$SiW_9O_{34}H$ lacunary structure further completed by 3 Mo atoms. The β-$SiW_{12}O_{40}$ structure differs from the Keggin α one by rotating one W_3O_{13} group by 60° under a ternary axis and in this case each WO_6 of this rotated group is sharing oxygen corners with WO_6 octahedra belonging to the same $W_{13}O_{13}$ group. As shown in the mixed HPA structure presenting three adjacent Mo octahedra, the initial β-$[SiW_9O_{34}H]$ structure was obtained by removing three adjacent W atoms from three different W_3O_{13} groups (that differ from the rotated W_3O_{13}) in agreement with the β-$[SiW_9O_{34}H]^{9-}$ structure reported by Robert and Tézé[37] and the α-$PMo_9O_{34}H_6{}^{3-}$ structure determined by Strandberg[38], showing in both cases three adjacent metallic sites. Based on these literature data, Sanchez et al.[9] assumed that in the β $SiMo_3W_9O_{40}{}^{4-}$ the three Mo atoms belonged to three different groups without performing any structural determination.

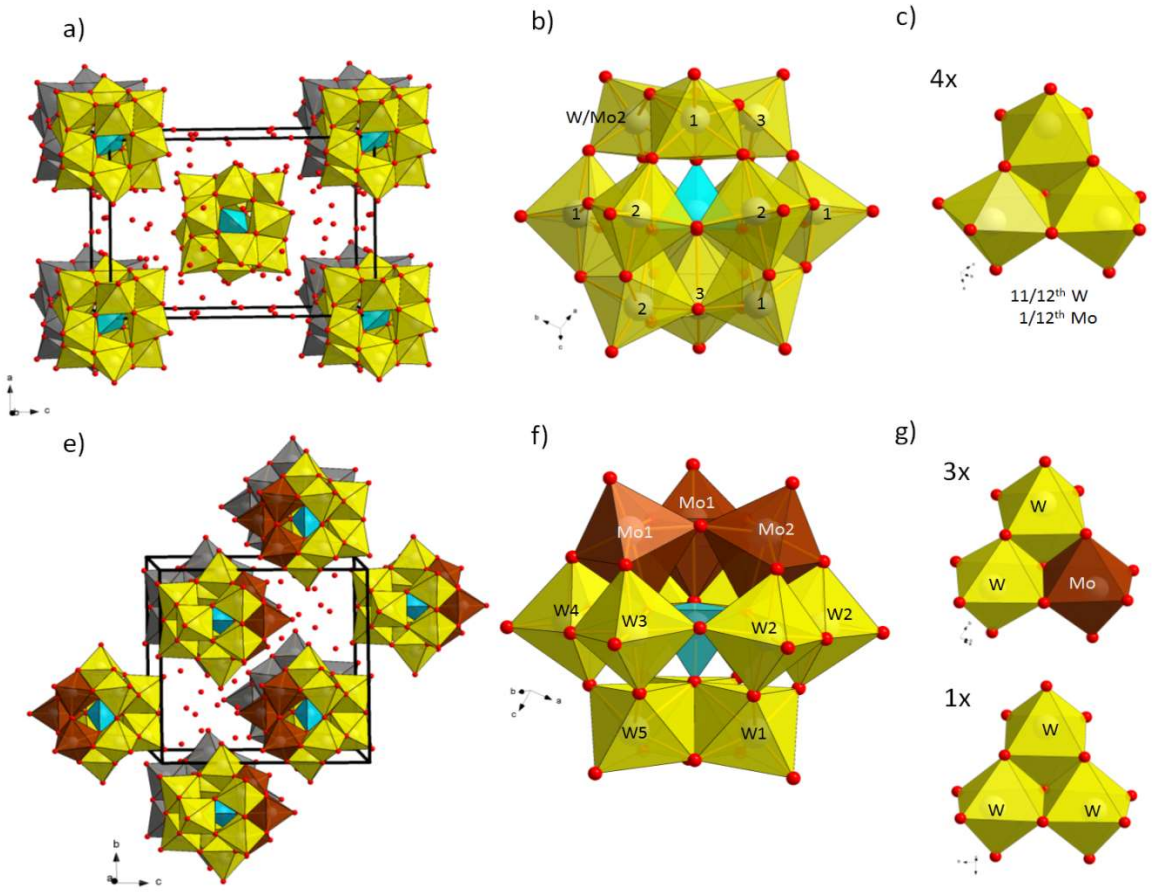

Figure 1. Crystals and detailed heteropolyanion structures and formation of α-$H_4[SiMo_1W_{11}O_{40}]$ (a,b,c) and β-$H_4[SiMo_3W_9O_{40}]$ (d,e,f,g).

Bulk HPA analysis

EXAFS analysis of bulk HPA

$H_4[SiMo_3W_9O_{40}]$

β-$H_4[SiW_9Mo_3O_{40}]$ EXAFS oscillations both at the Mo K and at the W L_{III} edges have been successfully refined (see supporting information) taking into account the radial distribution functions of neighbors deduced from the crystallographic data determined from XRD single crystal analysis. In Tables 3 and 4 are reported the main parameters of the least square fitting process at the Mo K and W L_{III} edges, the number of neighbors N, the distance R (Mo-X for Table 3 and W-X for Table 4), the Debye-Waller factor σ^2 and the R factor which measures the relative misfit of the simulation with the experimental data. In agreement with N and R crystallographic data also reported in Table 3 the first shell around the Mo atom contains three contributions due to three Mo-O different distances (1.68, 1.91, 2.38 Å) resulting from a distorted oxygen octahedral coordination whereas the second shell contains the contribution of W, Si and Mo backscattering neighbors at 3.40, 3.58 and 3.81 Å respectively. The second neighbors at 3.40 Å are W atoms from the same M_3O_{13} group while Mo neighbors belonging to another M_3O_{13} appeared at higher distance (3.81 Å). Around W (Table 4), the first coordination shell of bulk $H_4[SiW_9Mo_3O_{40}]$ presents similar oxygen contributions than that observed around Mo due to similar size of six-fold coordinated Mo^{6+} (0.59 Å) and W^{6+} (0.60 Å) cations[39]. The second coordination shell around W contains five contributions, the second neighbors around W are shared between W (N=1.33) and Mo (N=0.66) at 3.36 and 3.40 Å from the same M_3O_{13} group while W neighbors belonging to another M_3O_{13} group are shared between W from the 60° rotated W_3O_{13} group and the three others groups leading to two different distances equal to 3.74 Å and 3.68 Å respectively.

Journal Name

ARTICLE

Table 3. Structural parameters determined by least square fitting of the inverse Fourier Transform (ΔR = 1-3.9 Å) of the Mo K edge EXAFS signals for bulk $H_4[SiW_9Mo_3O_{40}]$ and $H_4[SiW_{11}Mo_1O_{40}]$ HPAs and their corresponding dried supported catalysts with S_0^2=1.0 and enot = 8.70 eV for a E_0 value used for EXAFS extraction equal to 20012.6 eV. Values given in bracket correspond to the values range determined from single crystal XRD data. Italic parameters were kept fixed during the minimization process.

Backscatterer	*N*	R (Å)	σ^2 x 10^3 (Å^2)	R-factor
		Bulk $H_4[SiMo_3W_9O_{40}]$		
O	*1.0 (1)*	1.68 *(1.67)*	1.7	0.0076
O	*4.0 (4)*	1.91 *(1.87-2.00)*	10.1	
O	*1.0 (1)*	2.38 *(2.37-2.39)*	0.5	
W	*2.0 (2)*	3.40 *(3.35-3.37)*	6.3	
Si	*1.0 (1)*	3.58 *(3.55-3.57)*	2.0	
Mo	*2.0 (2)*	3.81 *(3.72-3.78)*	4.3	
		$SiMo_3W_9/Al$		
O	*3.0*	1.75	7.0	0.0027
O	*2.0*	2.02	1.0	
O	*1.0*	2.37	1.5	
W	*2.0*	3.42	10.6	
Si	*1.0*	3.60	5.9	
Mo	*2.0*	3.82	13.3	
		Bulk $H_4[SiMo_1W_{11}O_{40}]$		
O	*3.0 (3)*	1.79 (*1.66-1.85)*	17.2	0.0259
O	*3.0 (3)*	2.00 *(1.95-2.40)*	2.7	
W	*4.0 (4)*	3.47 *(3.51-3.53)*	5.1	
Si	*1.0 (1)*	3.49 (*3.52-3.53)*	3.5	
		$SiMo_1W_{11}/Al$		
O	3.3	1.74	4.0	0.0670
O	2.7	1.96	3.9	
W	*4.0*	3.40	5.5	
Si	*1.0*	3.32	5.5	

Journal Name

ARTICLE

Table 4. Structural parameters-determined by least square fitting of the inverse Fourier Transform (ΔR = 1-4 Å) of the W L_{III} edge EXAFS signals for bulk $H_4[SiW_9Mo_3O_{40}]$ HPA and its corresponding dried supported catalyst with S_0^2=0.76 and enot = 8.6 eV for a E_0 value used for EXAFS extraction equal to 10206.70 eV. Values given in bracket correspond to the values range determined from single crystal XRD data. Italic parameters were kept fixed during the minimization process.

Backscatterer	N	R (Å)	σ^2 x 10^3 (Å^2)	R-factor
		Bulk $H_4[SiMo_3W_9O_{40}]$		
O	1.0 *(1)*	1.69 *(1.69-1.73)*	1.1	0.1290
O	4.0 *(4)*	1.90 *(1.88-1.94)*	5.0	
O	1.0 *(1)*	2.29 *(2.30-2.36)*	2.5	
W	1.33 *(1.33)*	3.36 *(3.30-3.36)*	6.3	
Mo	0.66 *(0.66)*	3.40 *(3.35-3.37)*	7.8	
Si	1.0 *(1)*	3.51 *(3.50-3.55)*	0.2	
W	1.33 *(1.33)*	3.68 *(3.64-3.66)*	4.4	
W	0.66 *(0.66)*	3.74 *(3.71-3.74)*	2.1	
		$SiMo_3W_9$/Al		
O	1.0	1.72	0.7	0.1111
O	4.0	1.89	5.5	
O	1.0	2.32	4.7	
W	1.33	3.36	6.6	
Mo	0.66	3.48	5.2	
Si	1.0	3.51	5.3	
W	1.33	3.65	4.1	
W	0.66	3.77	3.2	

$H_4[SiMo_1W_{11}O_{40}]$

α-$H_4[SiMo_1W_{11}O_{40}]$ EXAFS oscillations at the Mo K edge have also been successfully refined (see supporting information (SI)) using the radial distribution function extracted from crystallographic data deduced from XRD single analysis. In Table 3 the disordered octahedral coordination of Mo is described with two contributions of three oxygen neighbors at 1.79 and 2.00 Å. At the W L_{III} edge, due to the α symmetric structure, in addition to the Si contribution, only a unique W contribution at 3.47 Å is present in the second coordination shell. It was not possible to refine EXAFS oscillations at the W L_{III} edge for distances above the first coordination shell by keeping R and N crystallographic values. In this symmetric α structure, the part of multiple scattering is so important that a high contribution of paths involving at least 3 atoms as W-O-W has to be taken into account making the parameters to fit higher than the number of independent points in the fit.
These EXAFS results confirmed the formation of the mixed HPA.

IR, Raman and TGA-DSC analysis (SI)

IR and Raman spectra of $H_4[SiMo_1W_{11}O_{40}]$, $H_4[SiMo_3W_9O_{40}]$, $H_4[SiMo_{12}O_{40}]$ and $H_4[SiW_{12}O_{40}]$ are reported in SI. The IR spectra as well as the Raman ones of mixed HPA are very close and look like that of $H_4SiW_{12}O_{40}$ indicating that in the mixed HPA Mo- and W-oxygen vibrational modes cannot be observed separately. TGA-DSC analysis (see SI) shows that the thermal behavior of the mixed HPA and silicotungstic acid is very similar and that the substitution of W by Mo slightly decreases the thermal stability of the mixed HPA compared to that of silicotungstic acid.

HPA impregnating solutions analysis

Synthesis of mixed MoW HPA was devoted to the preparation of aqueous impregnating solutions for the preparation of MoW hydrotreatment catalysts possessing a MoW nanoscale proximity. It was then a key point to check the preservation of mixed heteropolyacids after their dissolution in water.

Raman spectroscopy

Raman spectra of impregnating solutions (Fig. 2) are in good agreement with those of the corresponding bulk compounds reported in SI. The similarity between the Raman spectra of the solid and of the solution of mixed HPA indicates i) the purity of the mixed solids with no formation of separate monometallic heteropolyanion and ii) their preservation after dissolution in water. As for Raman characterization at the solid state, the wavenumber of $M=O_t$ vibration (main peak of the Raman spectrum) corresponds to a weighted average of the $Mo=O_t$ and $W=O_t$ wavenumbers.

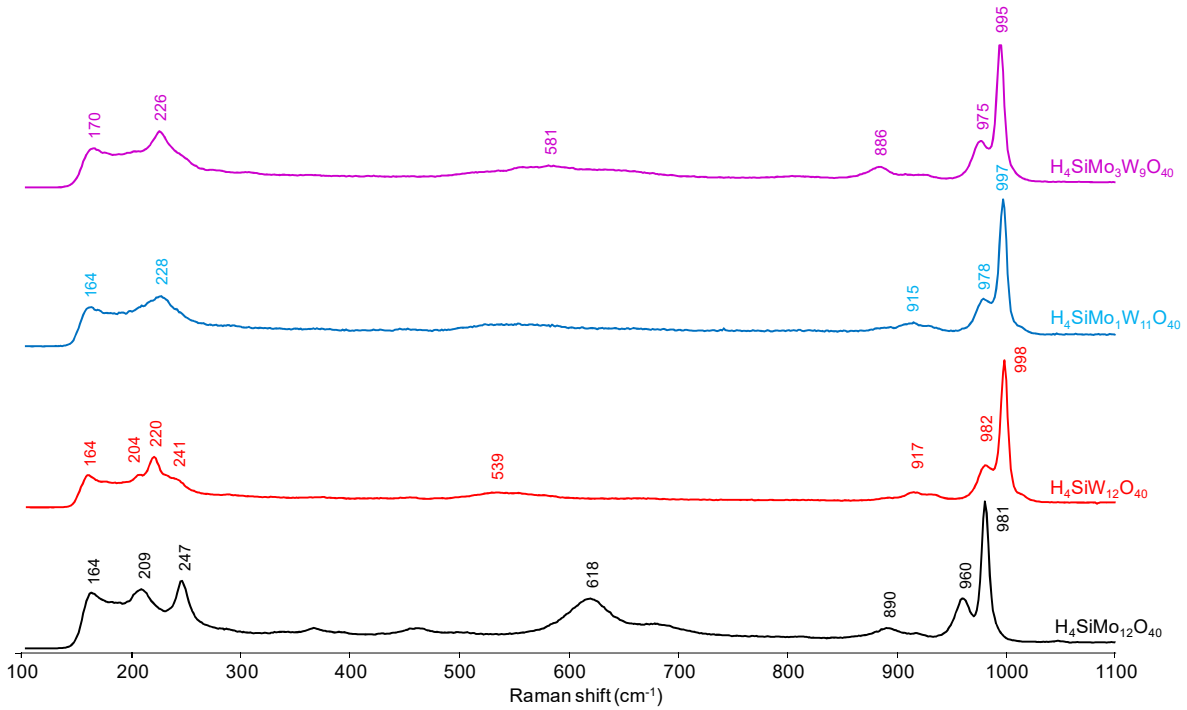

Figure 2. Raman spectra of HPA based impregnating solution.

Polarography

The electrochemistry of heteropolycompounds in solution has been studied for a long time by polarography.[2,3,40] It consists in observing the reduction waves (current (I)-potential (E) curves) corresponding to successive electron exchanges. In this work, due to the use of the glassy carbon disk as working electrode, the polarogram of $H_4SiW_{12}O_{40}$ solution where reduction waves appear between -0.3 and -1.0 V [28] cannot be observed. Fig. 3 shows the polarograms of the three HPA solutions obtained by dissolving bulk $H_4SiMo_{12}O_{40}$, $H_4SiMo_1W_{11}O_{40}$ and $H_4SiMo_3W_9O_{40}$ in a buffer medium. In the Keggin- like structure the electrons are delocalised over the entire polyanion, and Mo-O-Mo bridges allow the paired electrons to move according to the bipolaron model[9].The degrees of reduction of the heteropolymolybdates are referred to as 0, II, IV, VI… in which the roman number indicates that the anion is reduced by 0, 2, 4, 6 electrons or more. In acidic medium, three "2-electron" reduction waves (O-II, II-IV, IV-VI) can be seen in the polarogram of $H_4SiMo_{12}O_{40}$ under our experimental conditions (AgCl/Ag reference electrode and HCl 1 $mol.L^{-1}$/ethanol 50-50 vol electrolyte solution) with half-wave potentials recorded at 0.280, 0.190 and –0.020 V respectively. The global shape of the polarogram and the half-wave potentials values together with their differences are in agreement with literature data[1-3,28] and confirm the presence of α-$H_4SiMo_{12}O_{40}$ isomer. Polarography is one of the techniques allowing us to differentiate between α and β isomers (the first half-wave potential is expected around 0.380 V for the β-$H_4SiMo_{12}O_{40}$ isomer). For the two mixed HPA solutions, polarograms are clearly different from that of α-$H_4SiMo_{12}O_{40}$ and only one "2-electron" reduction wave (corresponding to the O-II) reduction is visible without any contribution of $H_4SiMo_{12}O_{40}$ anion. It means that all the waves are significantly shifted toward lower potential due to the presence of W in mixed HPA and the two other waves are shifted before -0.2 V and thus do not appear on the Figure 3. Taking into account that $H_4SiMo_3W_9O_{40}$ mixed HPA is a β isomer the presence of W greatly influences the Mo redox potential allowing to distinguish unambiguously between both mixed HPA. Moreover, the two well-defined polarograms of mixed samples indicate the presence of one type of HPA in solution in agreement with the existence of pure MoW mixed HPA.

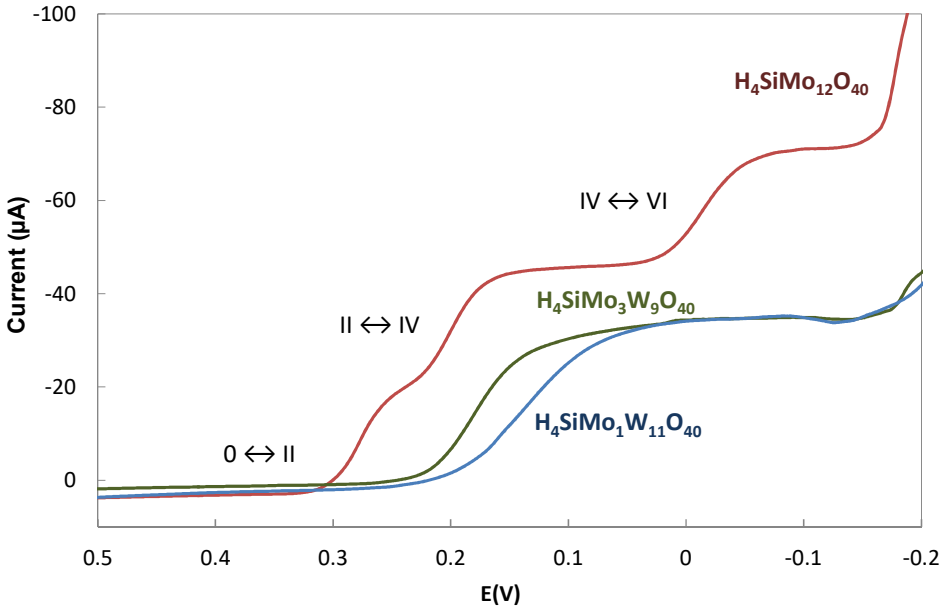

Figure 3. Polarograms of Mo containing HPA in 0.5 M ethanol/HCl mixture.

Characterization of supported oxidic precursors

Raman spectroscopy

To understand the behaviour of these HPA after deposition on the support, Raman spectra of catalysts after maturation and drying with that of the corresponding bulk HPA are reported on Fig. 4. Different behaviours depending on the catalyst can be observed. For $SiMo_{12}$/Al the spectrum of the solid after maturation does not correspond to that of the bulk $SiMo_{12}O_{40}^{4-}$ anion and new Raman lines are clearly observed at 948, 564, 350 and 215 cm^{-1}. These lines are unambiguously assigned to the formation of the well-known $AlMo_6O_{24}H_6^{3-}$Anderson heteropolyanion species that is formed through decomposition of $SiMo_{12}$ Keggin structure on the support due to the "buffer effect" of alumina and Al^{3+} extraction from the support[41,42]. This species is maintained after drying and well-dispersed on the alumina surface according to the broad Raman lines of the spectrum[11]. During impregnation the important parameter is the pH of the solution in the pore of alumina which evolves due to the PZC of alumina (around 7). The respective stability of tungsten and molybdenum based heteropolyacids in aqueous solutions at various pH have been studied in the literature demonstrating that tungsten based HPA are more stable than the molybdenum ones upon pH increase[3,43]. Indeed, tungsten containing catalysts show different behaviour since the spectra of the oxidic precursors are very similar to those of their bulk precursor. For the three W based catalysts, after maturation and drying only a shift (≈20 cm^{-1}) of the main line ($M=O_t$ vibration) towards lower wavenumbers is observed (from 1000 to 982 cm^{-1} for SiW_{12}/Al; from 998 to 979 cm^{-1} for $SiMo_1W_{11}$/Al and from 997 to 977 cm^{-1} for $SiMo_3W_9$/Al). Such shifts have already been observed after drying but in a lesser extent in the case of ASA supported heteropolytungstate and were attributed to interaction with the support[12]. Moreover, analysis of the low Raman shift region (below 260 cm^{-1}) shows similar lines in shape and position for the bulk and the corresponding maturated and dried W based HPA catalysts. The line around 220-230 cm^{-1} is attributed to the stretching mode of the W(Mo)-O vibration (where O links W(Mo) and Si) and is characteristic of Keggin structure[28]. The global Raman analysis of catalysts after maturation and drying suggests the preservation of the mixed MoW heteropolyanion species on alumina support even if the broadness of the Raman peaks could prevent a clear discrimination between SiW_{11} lacunary structure and $SiW_{11}Mo$ Keggin structure.

Journal Name

ARTICLE

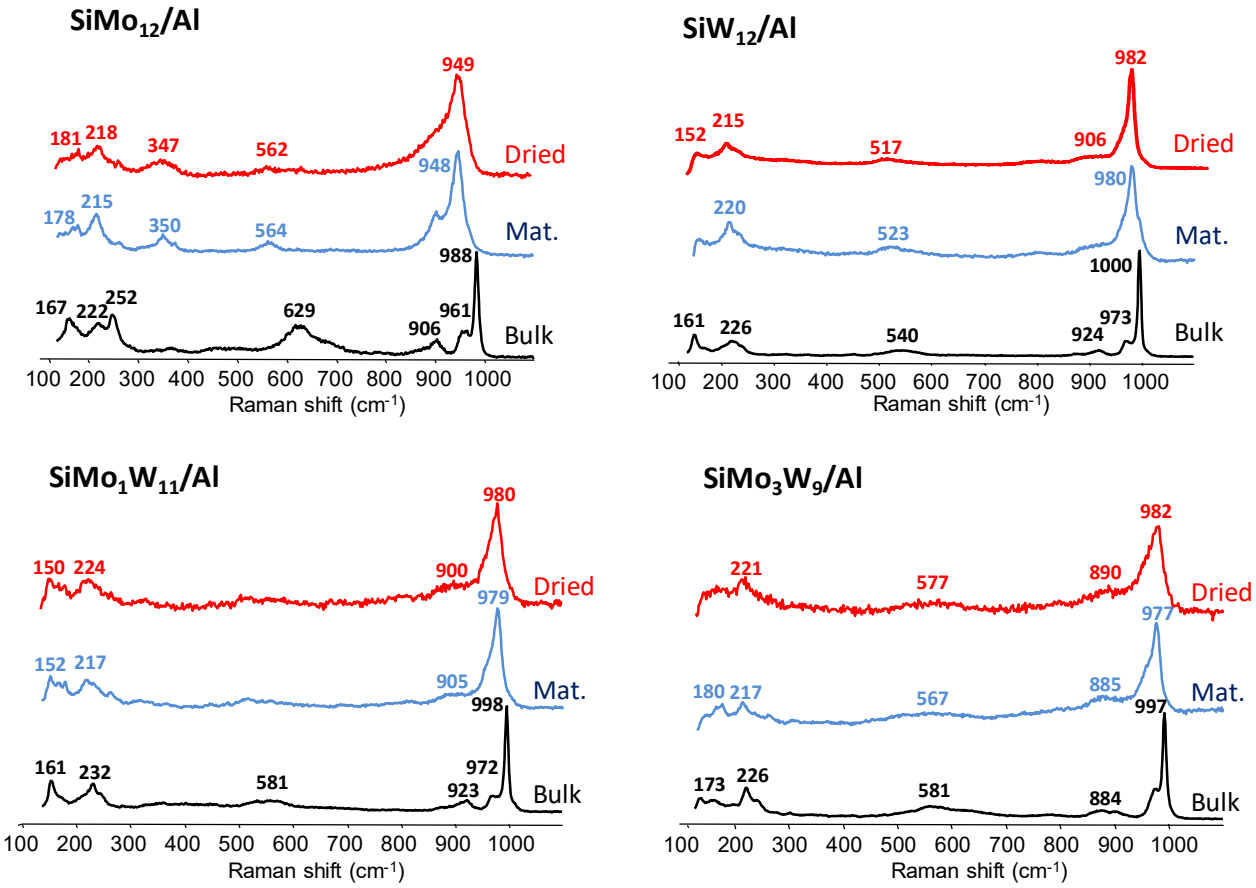

Figure 4. Raman characterisation of catalysts after maturation (Mat.) and drying (Dried) and their corresponding bulk HPA (Bulk).

EXAFS analysis

In order to confirm the preservation of the mixed HPA on alumina upon impregnation and drying, EXAFS experiments of dried catalyst have been performed at the W L_{III} and Mo K edges. For easier comparison purposes Fig. 5 reports EXAFS oscillations as well as Fourier Transform moduli at both edges for the dried catalysts and their corresponding bulk HPA. At the W L_{III} edge, Fig. 5 (a) and (b) show clearly that EXAFS signals and the corresponding Fourier transforms moduli of the dried samples $SiMo_1W_{11}/Al$ and $SiMo_3W_9/Al$ are both in phase with that of their corresponding mixed HPA. A successful fitting of $SiMo_3W_9/Al$ EXAFS data with crystallographic data of its bulk starting material has been then obtained and reported in Table 4 attesting that the local order around W is similar in the supported catalysts to the one of the bulk phase. This is a strong evidence of the preservation of this HPA on alumina after drying. As aforementioned, for $H_4SiMo_1W_{11}$ due to important multiple scattering contributions for this symmetric structure it was not possible to fit the EXAFS data at the W L_{III} edge. Nevertheless, from Fig. 5 (a) and (b) it is clear that the bulk starting HPA matches very well with its catalyst, indicating unambiguously it is maintained on alumina surface.

Regarding the Mo side (Fig. 5 (c) and (d)) if we compare dried catalysts with the bulk starting materials, similarities are observed in both EXAFS oscillations and FT even if the fitting results reported in Table 3 show some variations in the distances between Mo and its neighbours compared to that observed in the bulk materials. These results obtained from the Mo side could be explained by a partial decomposition of $SiMo_3W_9$ HPA with the removal of one Mo atom from the Keggin structure.

Journal Name

ARTICLE

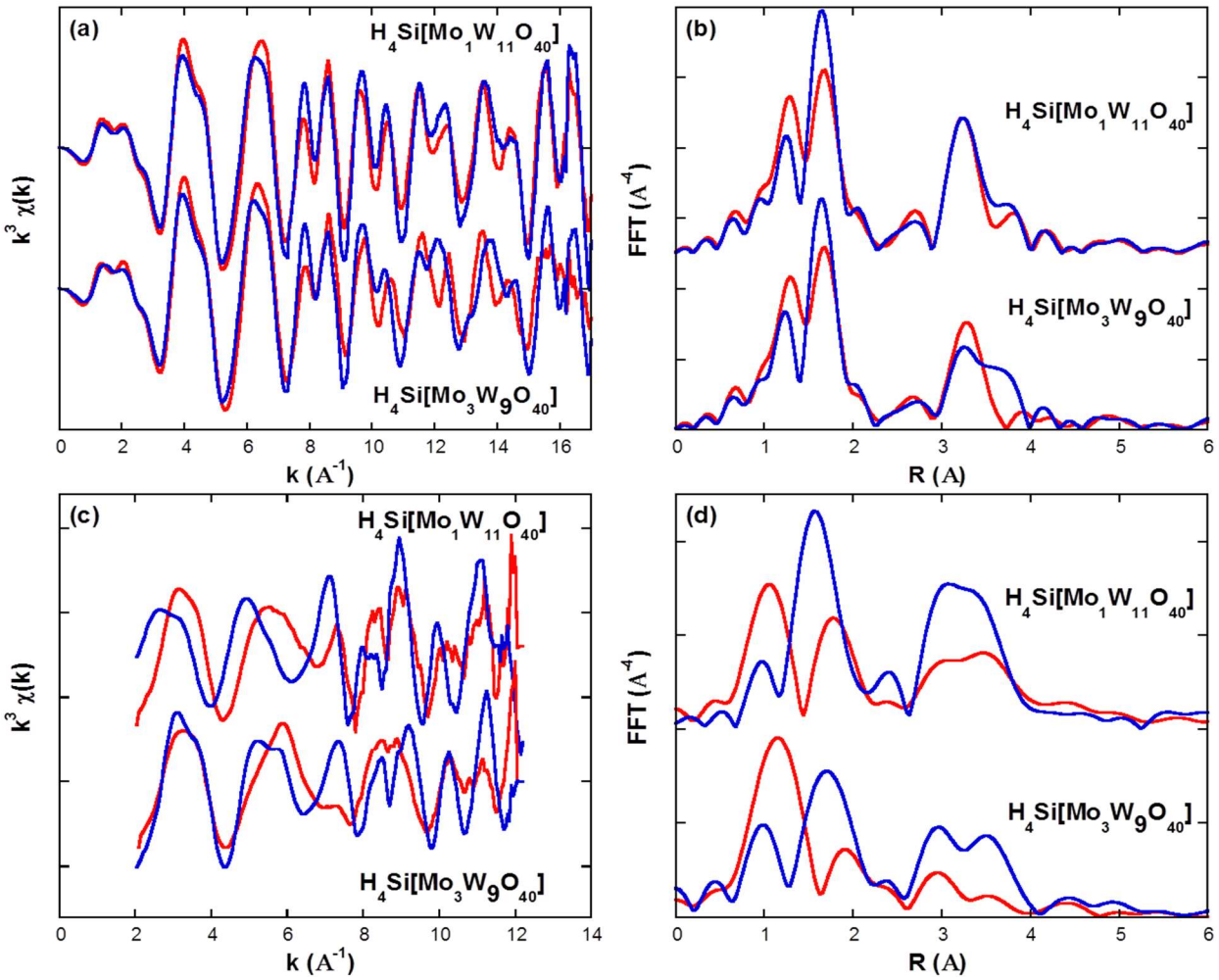

Figure 5. EXAFS oscillations at (a) W L_{III} edge, (c) Mo K edge and the corresponding Fourier Transform modulus at (b) W L_{III} edge (d) Mo K edge for dried mixed MoW catalyst in red and its bulk mixed HPA in blue.

Characterization of supported sulfide catalysts

EXAFS analysis

All prepared Mo(W)/Al catalysts were *in-situ* sulfided during synchrotron measurement sessions, with the same operating conditions than those used for activation of the solids prior to catalytic evaluation. The Fourier transform moduli data recorded for the samples at the end of the sulfidation are presented in Figure 6 and the corresponding fit EXAFS parameters are gathered in Table 5 and 7. At the Mo and W edges of all samples, the first contribution is located around 1.9 Å (phase-shift not corrected) on the FTs of the EXAFS signals and corresponds to S neighbors with a characteristic Mo-S or W-S distance equal to 2.41 Å, identical to that reported for bulk sulfided MoS_2 or WS_2 samples[44,22]. The second coordination shell, attributed to a metallic neighbor (Mo or W), is characterized by a distance around 3.17 Å, again identical to that of the bulk sulfide material[42,44]. Nevertheless, for this second contribution a significant change in magnitude is observed at both edges especially for the mixed catalyst compared to the monometallic ones. Slabs size of the MoS_2 or WS_2 phases could influence the magnitude of the second coordination shell, a decrease of the slabs size could be then reflected by the decrease N_{Mo-Mo} or N_{W-W} coordination number. Results of TEM characterization after liquid phase sulfidation showed

that $SiMo_{12}/Al$, SiW_{12}/Al and SiMo3W9/Al catalysts presented similar average slabs sizes with values of 4.7, 4.9 and 4.8 Å respectively[45]. It could be expected that gas sulfidation could also lead to similar average slabs length for these three catalysts. Nevertheless, besides the effect of dispersion (slab size) on the coordination number, the local ordering of the MoS_2 phase may also influence the coordination number and the introduction of some disorder (through the Debye-Waller factor) in the position of Mo atoms in a MoS2 slab can explain low Mo–Mo coordination numbers[46]. Moreover, the larger decrease observed for mixed HPA based catalysts could be due to the presence of W neighbors for Mo and *vice-versa*, that is due to the destructive interference of the individual scattering paths including either the absorbing atom and Mo or the absorbing atom and W which are out of phase[44,22].

It is thus necessary to fit the data to obtain reliable quantitative local coordination of Mo and W atoms (Table 5 and 6). For the Mo_xW_{12-x} solids, a Mo-W contribution had to be considered for an optimum fitting of the EXAFS spectra, with 2.9 and 1.5 W neighbors at the Mo edge and 0.7 and 1.5 Mo neighbors at the W edge, for $SiMo_1W_{11}/Al$ and $SiMo_3W_9/Al$ respectively. Contrariwise, introducing a Mo-W contribution does not improve the fitting in mixed MoW reference catalysts. Sulfide catalysts prepared from mixed heteropolyanions present Mo and W together closely coordinated which clearly demonstrates the quantitative formation of mixed Mo-W sulfide slabs. The formation of such mixed slabs may be favored by the nanoscale proximity of both metals in the heteropolyanionic structure. Recent literature discussed about mixed MoW disulfide phase formation when using different preparation and/or sulfidation procedures. Starting from separate Mo and W precursors to prepare bulk Ni promoted and unpromoted catalysts and using as sulfidation procedure 10 vol.% H_2S into H_2 under at 18 bar, Hein *et al.*[47,48] demonstrated by XAS the formation of mixed slabs from EXAFS refinements at the Mo K and W L_{III} edges. Haandel *et al.*[22] also deduced through EXAFS analysis mixed slabs formation for Ni-Mo-W catalysts prepared from conventional precursors and activated under gas sulfidation. This mixed phase has been recently clearly visualized for the first time thanks to HAADF images revealing through Z contrast W and Mo atoms in the same sulfide slabs[45]. This study was performed on $SiMo_3W_9/Al$ and its corresponding reference catalysts activated by liquid phase sulfidation and showed mixed $MoWS_2$ phase in both cases with the presence of monometallic slabs for the reference catalyst. In our case using gas sulfidation we can deduce predominant mixed sulfide phase formation using mixed HPA while monometallic WS_2 and MoS_2 phases are the main ones using separate monometallic HPA.

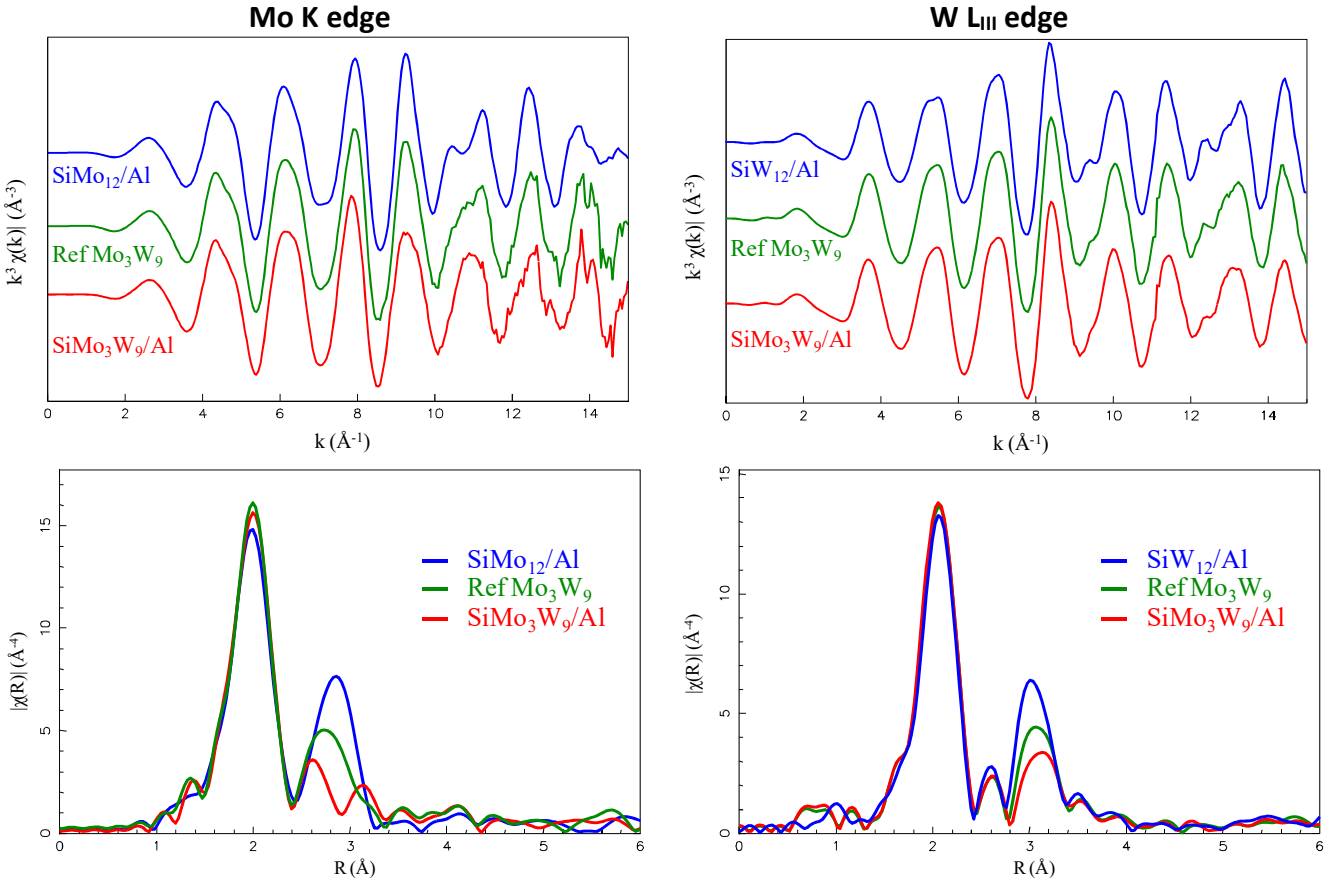

Figure 6. EXAFS at the Mo K edge and W L_{III} edge and the corresponding Fourier transforms of sulfided Mo(W)/Al catalysts.

Journal Name

ARTICLE

Table 5: Parameters obtained from the fit of the Mo K edge EXAFS spectra of the sulfided Mo(W)/Al catalysts at the Mo K edge (Δk=3.5-15 $Å^{-1}$, R-range 1.5-3.35 Å, S^2_0 = 1.05 and enot = 1.6 ± 2 eV for a E_0 value used for EXAFS extraction equal to 20004.3 eV).

Backscatterer	*N*	R (Å)	σ^2 x 10^3 ($Å^2$)	R-factor
$SiMo_{12}$/Al				
Mo-S	5.1 ± 0.2	2.41 ± 0.01	4.3 ± 0.3	0.0007
Mo-Mo	3.3 ± 0.3	3.17 ± 0.01	5.3 ± 0.4	
$SiMo_3W_9$/Al				
Mo-S	5.3 ±1.1	2.41 ±0.01	4.0 ±1.3	0.0111
Mo-Mo	1.3 ±0.8	3.16 ±0.02	3.7 ±2.1	
Mo-W	1.5 ±1.0	3.15 ±0.01	3.7 ±2.1	
Ref Mo_3W_9				
Mo-S	5.1 ±0.6	2.41 ±0.01	3.7 ±0.6	0.0081
Mo-Mo	3.5 ±1.7	3.17 ±0.01	7.8 ±2.8	

Table 6: Parameters obtained from the fit of the W L_{III} edge EXAFS spectra of the sulfided Mo(W)/Al catalysts at the W L_{III} edge (Δk=4.3-16.3 $Å^{-1}$, R-range 1.4-3.4 Å, S^2_0 = 0.87 and enot = 8.90 ± 2.0 eV for a E_0 value used for EXAFS extraction equal to 10218.8 eV).

Backscatterer	*N*	R (Å)	σ^2x 10^3 ($Å^2$)	R-factor
SiW_{12}/Al				
W-S	4.3 ±0.4	2.41 ±0.01	3.2±0.6	0.0091
W-W	3.0 ±0.6	3.16 ±0.007	4.3 ±0.8	
$SiMo_3W_9$/Al				
W-S	4.8 ±0.5	2.41 ±0.01	3.4 ±0.7	0.0111
W-W	1.7±0.9	3.17 ±0.01	3.7 ±2.1	
W-Mo	1.5 ±1.1	3.15 ±0.01	3.7 ±2.1	
Ref Mo_3W_9				
W-S	4.7 ±0.5	2.41±0.01	3.4 ±0.7	0.0106
W-W	2.6±0.9	3.16 ±0.01	4.7 ±1.4	

XPS

Figure 7 shows the decomposition of the Mo3d and the W4f spectra for sulfided $SiMo_{12}$/Al, SiW_{12}/Al, $SiMo_3W_9$/Al and Ref Mo_3W_9 catalysts. This decomposition allows to obtain the relative amounts of the different Mo and W species that are gathered in Table 7. The sulfidation rate corresponding to the MoS_2 atomic % is very high (above 80 %) in the three Mo containing catalysts, compared with sulfidation rate reported in the literature for conventional HDS catalysts (around 60 %)[49]. It shows that the molybdenum content varying from 4.2 to 18 MoO_3 wt % has no influence on the sulfidation rate. The Ref Mo_3W_9 catalyst possesses the highest MoS_2 sulfidation rate reaching 91 %. A low sulfidation degree of tungsten (49 %) is observed for SiW_{12}/Al catalyst that could be attributed to a strong W-O bond compared to the Mo-O one that could delay the formation of WS_2 phase compared to that of MoS_2 phase at a given sulfidation temperature[50,51]. The presence of Mo in catalyst formulation clearly leads to increase W sulfidation that reaches 61 and 67 % for $SiMo_3W_9$/Al and Ref Mo_3W_9 respectively.

Journal Name

ARTICLE

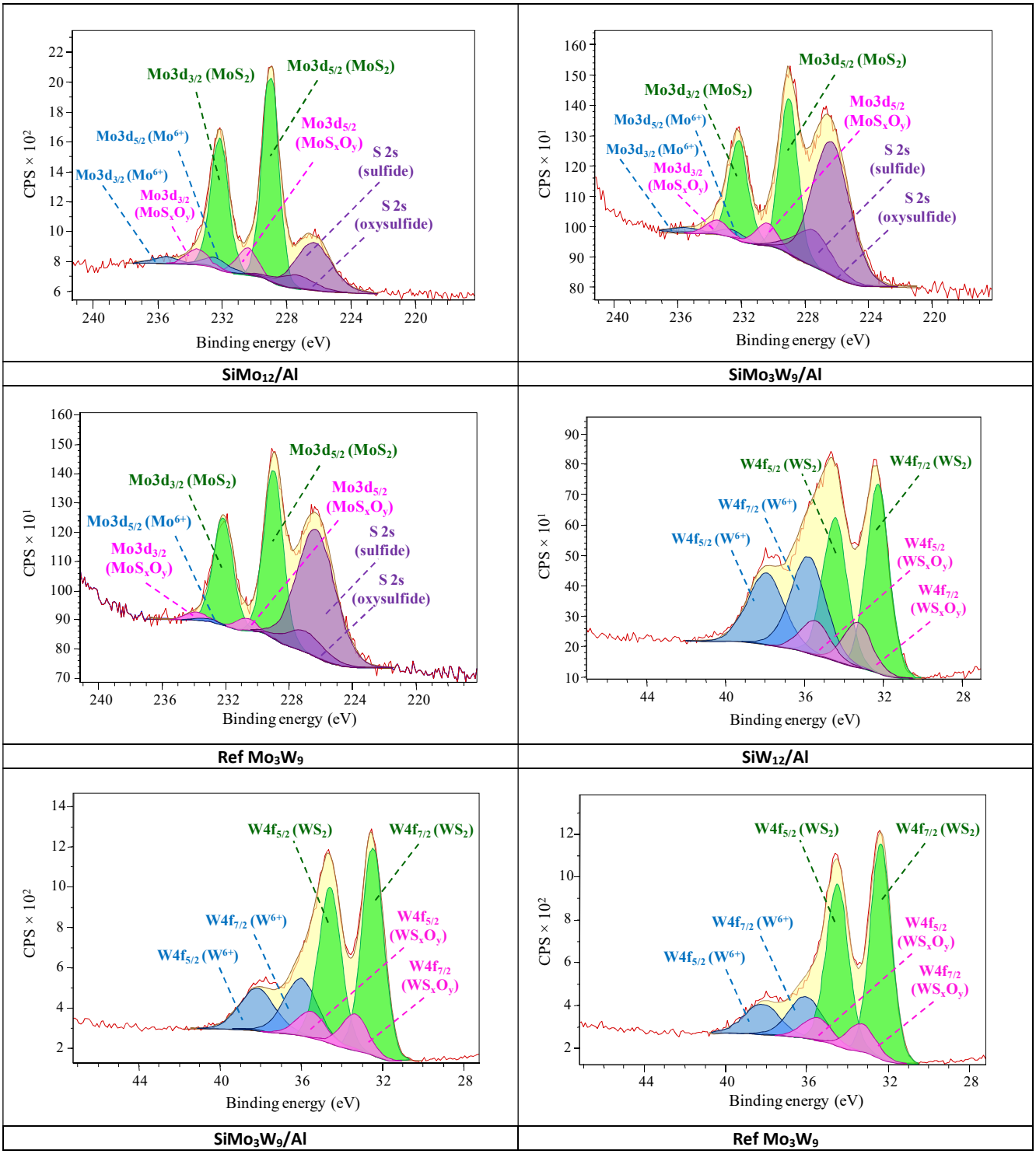

Figure 7. XPS Mo 3d and W 4f spectra recorded for Mo(W)/Al catalysts; in blue: $Mo(W)^{6+}$oxide contributions; in pink: $Mo(W)S_xO_y$ contributions; in green: $Mo(W)S_2$ contributions (For interpretation of the references to color in this figure legend, the reader is referred to the web version of the article).

Journal Name

ARTICLE

Table 7. Relative at.% of Mo and W species in sulfided Mo(W)/Al catalysts.

Catalysts	MoS_2	MoO_xS_y	Mo^{VI}	WS_2	WO_xS_y	W^{VI}
$SiMo_{12}/Al$	82	12	6	-	-	-
SiW_{12}/Al	-	-	-	49	14	37
$SiMo_3W_9/Al$	81	14	5	61	13	26
Ref Mo_3W_9	91	7	2	67	15	21

Table 8. Catalytic properties of prepared Mo(W)/Al catalysts in DBT HDS and naphthalene Hyd.

Catalysts	DBT HDS (%)	Selectivity ratio $S_{HYD}/_{DDS}$	Rate constant k_{HDS} ×10^{-5} (mol h^{-1} g^{-1})	Naphthalene Hyd (%)	Rate constant k_{Hyd} ×10^{-5} (mol h^{-1} g^{-1})
$SiMo_{12}/Al$	51.9	1.7±0.2	45.1	40.5±0.5	157.3
SiW_{12}/Al	22.2	2.6±0.2	15.5	23.8±0.3	82.4
$SiMo_1W_{11}/Al$	49.2	2.6±0.2	41.8 (17.9*)	42.6±0.4	168.6 (88.6*)
$SiMo_3W_9/Al$	52.9	3.2±0.4	46.4 (22.9*)	47.5±0.5	195.2 (101.1*)
Ref Mo_1W_{11}	20.6	2.9±0.3	14.2 (17.9*)	24.4±0.2	85.0 (88.6*)
Ref Mo_3W_9	32.1	1.8±0.2	23.9 (22.9*)	27.3±0.3	96.7 (101.1*)

*The additive quantities, which were calculated using the values for monometallic $SiMo_{12}/Al_2$ and SiW_{12}/Al

Catalytic results

Hydrotreatment (HDT) catalytic properties in dibenzothiophene (DBT) hydrodesulfurization (HDS) and naphthalene hydrogenation (Hyd) are reported in Table 8.

The conversion of the reactants over all catalysts largely vary from 20.6 to 52.9 % for dibenzothiophene HDS and from 23.8 to 47.5 % for naphthalene Hyd. Compared to SiW_{12}/Al, the presence of a small amount of molybdenum in Ref Mo_1W_{11} has no significant effect on both HDS and Hyd properties. However, replacement of three tungsten atoms by molybdenum in Ref Mo_3W_9 leads to an increase in the catalytic activity in HDS of DBT from 22.2 to 32.1 and from 23.8 to 27.3 in Hyd of naphthalene. Taking into account the Mo and W atomic ratio together with their corresponding sulfidation rates previously calculated by XPS, the HDS rate constant of Ref Mo_3W_9 catalyst (23.9 10^5 mol h^{-1} g^{-1}) is almost a linear combination between that of $SiMo_{12}/Al$ and SiW_{12}/Al (22.9 10^5 mol h^{-1} g^{-1} for the calculated value). Naphthalene hydrogenation rate constant of Ref Mo_3W_9 (96.7 10^5 mol h^{-1} g^{-1}) appears to be even lower than the calculated value (101.1 10^5 mol h^{-1} g^{-1}). When using a mixed heteropolyanionic precursor, the addition of Mo in the $SiMo_xW_{12-x}/Al$ catalysts has a large beneficial effect in both HDS and Hyd. HDS conversions are 49.2 % for $SiMo_1W_{11}/Al$ and 52.9 % for $SiMo_3W_9/Al$, reaching then the HDS performance of pure Mo catalyst (51.9 %) with four times less molybdenum.

Concerning Hyd ability, conversion of 42.6 % is obtained for $SiMo_1W_{11}/Al$ and of 47.5 % for $SiMo_3W_9/Al$, this later value being significantly higher than that measured for pure Mo catalyst (40.5 %). $SiMo_3W_9/Al$ catalyst thus demonstrates the highest activity in both studied reactions. Comparison of reaction rates between $SiMo_3W_9/Al$ and Ref Mo_3W_9 shows for the mixed HPA catalyst. a relative increase evaluated at 65 % in DBT HDS and 74 % in naphthalene hydrogenation. This observation supports the formation of a mixed Mo-W active phase developing different catalytic properties. The mixed HPA based catalyst also presents the highest selectivity ratio $S_{HYD/DDS}$ (Table 8), with a value of 3.2 showing that the presence of the mixed sulfide phase leads to improved hydrogenation properties. Such properties are required for the treatment of heavy fuels[52-54].

Mixed MoW catalysts have been studied by Thomazeau et al.[24] who prepared MoW catalysts by incipient wetness co-impregnation of alumina with solutions of separate precursors, ammonium heptamolybdate $(NH_4)_6Mo_7O_{24}$ and ammonium metatungstate $(NH_4)_6H_2W_{12}O_{40}$. They reported a continuous variation of the thiophene HDS activity for the alumina $Mo_{1-x}W_xS_2$ series, in agreement with the behaviour of separate MoS_2 and WS_2 phase as we noticed for Ref Mo_3W_9 catalyst. Other authors reported in the case of separate Mo and W precursors that the thiophene HDS

performance of Ni promoted mixed MoW with low Mo content (Mo/W≤1) were comparable to that of the catalysts containing only W, as we observed for our Ref Mo_1W_{11}[44].

Our catalytic results allow us to show that the origin of the catalytic improvement observed for Mo_xW_{12-x} is not only due to the simultaneous presence of Mo and W as in Ref catalysts but also arises from close interaction of both metals in the mixed HPA precursor leading to the formation of mixed $Mo_xW_{1-x}S_2$ active phase, as supported by XAS analysis.

Conclusions

In this study, mixed MoW heropolyacids α-$H_4[SiMo_1W_{11}O_{40}]$ and β-$H_4[SiMo_3W_9O_{40}]$ have been synthesized from their corresponding mixed potassium salts starting from mono and tri-vacant heteropolytungstates. Crystallographic structures have been obtained and the corresponding data were used to fit with success EXAFS oscillations at the Mo K edge showing typical Mo-W distances for both mixed heteropolyacids. The purity of the samples was checked by characterizations at the liquid state using Raman spectroscopy and polarography. These mixed HPA were used for preparing hydrotreatment catalysts. After deposition on alumina, mixed HPA seems to be preserved even if a partial decomposition to lacunary Keggin species may occurs and their use ensure the nanoscale proximity between Mo and W. This close vicinity between Mo and W explains the formation after sulfidation of mixed MoW sulfide slabs for mixed HPA based catalysts as demonstrated by EXAFS fitting at the Mo K and W L_{III} edges. Catalytic performances in dibenzothiophene HDS and naphthalene hydrogenation have been evaluated. Catalytic results confirm the beneficial use of mixed HPA and particularly β-$H_4[SiMo_3W_9O_{40}]$ compared to the use of a mixture of monometallic Mo and W HPA precursors. Higher hydrogenation properties are explained by the mixed $(MoW)S_2$ active phase formation.

Conflicts of interest

There are no conflicts to declare.

Acknowledgements

Chevreul Institute (FR 2638), Ministère de l'Enseignement Supérieur et de la Recherche, Région Nord – Pas de Calais and FEDER are acknowledged for supporting and funding partially this work. This work was supported by a public grant overseen by the French National Research Agency(ANR) as part of the "Investissements d'Avenir" program (reference: ANR-10-EQPX-45) as well as the Kolmogorov PHC (project number 38175WC). The work was also supported the Ministry of Education and Science of the RF under project No. 14.586.21.0054 (project unique identifier RFMEFI58617X0054). M. Nikulshina thanks French Embassy in Russia for the Vernadsky fellowship and Haldor Topsøe Company for the grant to perform PhD thesis.

Supporting Information Available: Intra HPA cation-anion bond distances. Bulk $H_4[SiMo_1W_{11}O_{40}]$ and $H_4[SiMo_3W_9O_{40}]$ EXAFS oscillations at the Mo K and at the W L_{III} edges: FIT and experimental data. X-Ray crystallographic files (CIF). Bulk $H_4[SiMo_1W_{11}O_{40}]$, $H_4[SiMo_3W_9O_{40}]$, $H_4[SiMo_{12}O_{40}]$ and $H_4[SiW_{12}O_{40}]$ IR and Raman spectra and TGA-DSC analysis.

Notes and references

1 J. F. Keggin, *Proc. Royal Soc. A,* 1934, **144**, 75-100.
2 V. M. T. Pope, Heteropoly and Isopoly Oxometalates. *Springer-Verlag* 1983, **XIII**, 180 S., geb. DM 124.00.
3 P. Souchay, *Ions minéraux condensés,* Masson et Cie 1969.
4 J.F. Keggin, *Nature,* 1933, **131**, 908-909.
5 N. Mizuno and M. Misono, *J. Mol. Catal.,* 1994, **86**, 1-3, 319-342.
6 G. M. Brown, M. R. Noe-Spirlet, W. R. Busing and H. A. Levy, *Acta. Cryst.,* 1977, **B33**, 1038-1046.
7 A. Téazéa, G. Hervéa, R. Finke, G. David and K. Lyon, *Inorg. Synth.* 1990, **27**, 85-96.
8 P. Courtin, *Rev. Chim. Min.,* 1971, **8**, 75.
9 C.Sanchez, J.Livage, J.P.Launay, M.Fournier and Y.Jeannin, *J. Am. Chem. Soc.,* 1982, **104**, 11, 3194-3202.
10 Y. Shen, J. Peng, Z. Huanqiu, X. Yu and A. M. Bond, *Inorg. Chem.,* 2012, **51**, 5146–5151.
11 P. Blanchard, C. Lamonier, A. Griboval and E. Payen, *Appl. Catal. A Gen.,* 2007, **322**, 33-45.
12 K. Ben Tayeb, C. Lamonier, C. Lancelot, M. Fournier, E. Payen, A. Bonduelle and F. Bertoncini, *Catal. Today,* 2010, **150**, 207-212.
13 P. Nikulshin, A. Mozhaev, C. Lancelot, P. Blanchard, E. Payen and C. Lamonier, *C. R. Chimie,* 2016, **19**, 1276-1285.
14 P. Nikulshin, D. Ishutenko, Yu. Anashkin, A. Mozhaev, A. Pimerzin, *Fuel* 2016, **182**, 632–639.
15 D. Ishutenko, P. Nikulshin and A. Pimerzin, *Catal. Today,* 2016, **271**, 16–27.
16 D. Soogund, B. Guichard, A. Daudin, C. Lamonier and E. Payen, *Appl. Catal. B Env.,* 2010, **98**, 39-48.
17 N. Tomina, P. Nikul'shin and A. Pimerzin, *Pet. Chem.,* 2008, **48**, 92-99.
18 A. Griboval, P. Blanchard, E. Payen, M. Fournier, J.L. Dubois and J.R. Bernard, *Phosphorus research bulletin,* 1999, **10**, 436-441.
19 K. Ben Tayeb, C. Lamonier, C. Lancelot, M. Fournier, A. Bonduelle-Skrzypczak and F. Bertoncini, *Appl. Catal. B Env.,* 2012, **126**, 56-63.
20 S. Eijsbouts, F. Plantenga, B. Leliveld, Y. Inoue and K. Fujita, *Prepr. Pap.-Am. Chem. Soc., Div. Fuel Chem.* 2003, **48(2)**, 494-495.
21 S.L. González-Cortés, S. Rugmini, T. Xiao, M.L.H. Green, S.M.

Rodulfo-Baechler and F.E. Imbert, *Appl. Catal. A Gen.*, 2014, **475**, 270–281.
22 L. V. Haandel, M. Bremmer, P. J. Kooyman, J. A Rob van Veen, T. Weber and E. J. M. Hensen, *ACS Catal.*, 2015, **5**, 7276-7287.
23 C. Thomazeau, C. Geantet, M. Lacroix, M. Danot, V. Harle and P. Raybaud, *Appl. Catal. A Gen.,* 2007, **322**, 92–97.
24 C. Thomazeau, C. Geantet, M. Lacroix, V. Harle, S. Benazeth, C. Marhic and M. Danot, *Journal of Solid State Chemistry,* 2001, **160**, 147–155.
25 J. A. Mendoza-Nieto, O. Vera-Vallejo, L. Escobar-Alarcón, D. Solís-Casados and T. Klimova, *Fuel,* 2013, **110**, 268–277.
26 A. Tézé and G. Hervé, *J. inorg. nucl.Chem.,* 1977, **39**, 999-1002.
27 G. Hervé and A. Tézé, *Inorg. Chem*., 1977, **16**, 8, 2115-2117.
28 C. Rocchiccioli-Deltcheff, M. Fournier, R. Franck and R. Thouvenot, *Inorg. Chem.*, 1983, **22**, 207-216.
29 G. Sheldrix, SADABS: Area Detector Absorption Correction, Madison: WI, 1996.
30 L. Palatinus and G. Chapuis, *J. Appl. Cryst.*, 2007, **40**, 786-790.
31 V. Petricek, M. Dusek and L. Palatinus, *Kristallogr.*, 2014, **229(5)**, 345-352.
32 V. Briois, C. La Fontaine, S. Belin, L. Barthe, T. Moreno, V. Pinty, A. Carcy, R. Girardot and E. Fonda, JPCS 712, 2016**,** 1-6.
33 C. La Fontaine, L. Barthe, A. Rochet and V. Briois, *Catal. Today,* 2013, **205**, 148–158.
34 B. Ravel and M. Newville, *J. Synchrotron Radiat.,* 2005, **12**, 537–541.
35 E. A. Stern, *Phys. Rev. B*., 1993, **48**, 9825-9827.
36 A. Cordova, P. Blanchard, C. Lancelot, G. Frémy and C. Lamonier, *ACS Catal.,* 2015, **5**, 2966-2981.
37 F. Robert and A. Tézé, *Acta Cryst.,* 1981, **B37**, 318-322.
38 R. Strandberg, *Acta Chem. Scand*., 1974, **A28**, 217-225.
39 R. D. Shannon, *Acta Cryst.,* 1976, **A32**, 751-767.
40 P. Souchay, Polyanions et Polycations. *Gauthier Villars éditeur*, Paris, 1963.
41 L. Le Bihan, P. Blanchard, M. Fournier, J. Grimblot and E. Payen, *J. Chem. Soc. Faraday Trans.,* 1998, **94**, 937-940.
42 X. Carrier, J. F. Lambert and M. Che, *J. Am. Chem. Soc.,* 1997, **119**, 10137-10146.
43 A. Jürgensen and J. B. Moffat, *Catal. Lett.,* 1995, **34**, 237–244.
44 A. Rochet, B. Baubet, V. Moizan, E. Devers, A. Hugon, C. Pichon, E. Payen and V. Briois, *J. Phys. Chem. C* 2015, **119**, 23928-23942.
45 M. Nikulshina, A. Mozhaev, C. Lancelot, M. Marinova, P. Blanchard, E. Payen, C. Lamonier and P. Nikulshin, *Appl. Catal. B Env.,* 2018, **224**, 951–959.
46 E. J. M. Hensen, P. J. Kooyman, Y. van der Meer,A. M. van der Kraan, V. H. J. de Beer, J. A. R. van Veen, and R. A. van Santen, *J. Catal., 2001, **199**, 224–235*
47 J. Hein, O. Y. Gutiérrez, E. Schachtl, P. Xu, N. D. Browning, A. Jentys and J. A. Lercher, *ChemCatChem*, 2015, **7**, 3692-3704.
48 J. Hein, O. Y. Gutiérrez, S. Albersberger, J. Han, A. Jentys and J. A. Lercher, *ChemCatChem*, 2017, **9**, 629-641.
49 P. Blanchard, N. Frizi, S. Mary, P. Baranek, C. Lancelot, C. Lamonier and E. Payen, *C. R. Chim.*, 2016, **19**, 1286-1302.
50 A. J. Van des Vlies R. Prins and T. Weber, *J. Phys. Chem. B* 2002, **106**, 9277-9285.
51 M. J. Vissenberg, L. J. M. Joosten, M. M. E. H. Heffels, A. J. van Welsenes, V. H. J. de Beer, R. A. van Santen and J. A. R. van Veen, *J. Phys. Chem. B,* 2000, **104**, 8456-8461.
52 A. Varakin, P. Nikul'shin, A. Pimerzin, V. Sal'nikov and A. Pimerzin, *Rus. J. of Appl. Chem.,* 2013, **86**, 718-726.
53 T. C. Ho and J.M. McConnachie, *J. Catal.,* 2011, **277**, 117–122.
54 S. L. Amaya, G. Alonso-Núnez, T.A. Zepeda, S. Fuentes and A. Echavarría, *Appl. Catal. B Env.,* 2014, **148–149**, 221– 230.